

Structural Insights for Molecular Design of Conjugated Molecule and Polymers

by

Brandon Wood

A dissertation submitted in partial satisfaction of the

requirements for the degree of

Doctor of Philosophy

in

Applied Science and Technology

in the

Graduate Division

of the

University of California, Berkeley

Committee in charge:

Associate Professor Kristin Persson, Chair

The Aldo DeBenedictis Distinguished Professor Phillip Geissler

Professor Daryl Chrzan

Summer 2019

The dissertation of Brandon Wood, titled Structural Insights for Molecular Design of Conjugated Molecule and Polymers, is approved:

Chair _____

Date _____
Date _____
Date _____

University of California, Berkeley

Structural Insights for Molecular Design of Conjugated Molecule and Polymers

Copyright 2019
by
Brandon Wood

Abstract

Structural Insights for Molecular Design of Conjugated Molecule and Polymers

by

Brandon Wood

Doctor of Philosophy in Applied Science and Technology

University of California, Berkeley

Associate Professor Kristin Persson, Chair

Abstract will go here

To Mom

Contents

Contents	ii
List of Figures	iii
List of Tables	vi
1 Introduction	1
2 Structural Changes in Doped and Excited Conjugated Polymers	2
3 Aromaticity as a Guide to Planarity in Conjugated Molecules and Polymers	3
3.1 Introduction	3
3.2 Results and Discussion	4
3.3 Conclusion	8
3.4 Computational Methods	8
4 Conclusion	10
Bibliography	11
A Appendix for Aromaticity as a Guide to Planarity in Conjugated Molecules and Polymers	15
A.1 Different Length Polymer Chains	15
A.2 Comparision of MCI and NICS Aromaticity Values	18
A.3 Through-space Calculations	21

List of Figures

- 3.1 Ring aromaticity, molecular conjugation, and relative energies are plotted as a function of torsion angle for bithiophene (BT) and hydrogenated bithiophene (hBT). Both BT and hBT structures are represented in the 180° (trans) configuration. Aromaticity and conjugation are directly opposed in BT and the balance between the two driving forces results in a non-planar torsional minimum around 150°. Hydrogenation of the terminal C-C double bonds essentially reduces aromaticity to zero, while preserving conjugation across the two rings. With aromaticity removed in hBT, torsional energetics mirror conjugation and there is a planar minimum at 180°. Aromaticity is defined as the multicenter bonding index ($MCI \times 10^3$) for one C-C-S-C-C thiophene ring. Only one ring is displayed because both BT and hBT are symmetric molecules. Conjugation is quantified as the normalized relative bridge C-C bond length. A value of 1 represents the shortest bond length and the highest conjugation, whereas 0 represents the longest bond and lowest amount of conjugation.
- 5
- 3.2 (Top) Torsional relative energies and aromaticity are plotted for F2-BT and BEDOT. In both systems aromaticity is increased near 180° and this corresponds to an energetic minimum. (Bottom) Ring 1 and ring 2 aromaticities are plotted against torsion angles for BT, 3F-BT, and 4F-BT. Both rings are plotted because 3F-BT and 4F-BT molecules are no longer symmetric as is BT. For ring 1 the addition of F—regardless of the position—reduces the magnitude of aromaticity by a constant, but preserves the shape of the BT curve. The ring 2 curves are similar for 4F-BT and BT, however, ring 2 of 3F-BT deviates in shape and aromaticity is increased near 180° similar to the plots in the top of figure.
- 6
- 3.3 (Top) Isosurface plots of the overlap between C-S antibonding (σ_{C-S}^*) and F or O lone pair (LP) natural bonding orbitals in F2-BT and EDOT (isovalue ≈ 0.03). The orbital overlap leads to a stabilizing hyperconjugation interaction depicted in between the isosurface plots. (Bottom) The torsion potentials of F2-BT and BEDOT are displayed for ω B97x-D, RHF, and RHF with the σ_{C-S}^* orbital removed. RHF and ω B97x-D are qualitatively similar, both having a minimum at 180°. When the σ_{C-S}^* orbital is deleted from the Fock matrix (using NBO6) the hyperconjugative stabilization is no longer present and without that interaction the molecules are no longer planar.
- 7

A.1	Different length oligomers of thiophene.	15
A.2	The torsion potential of N2, N4, and N8 thiophene oligomers. All calculations were performed using the ω B97x-D functional. The N2 torsion potential was calculated with the def2-TZVPP basis set, while N4 and N8 utilized the 6-31++G**[19] basis set to reduce to the computational cost. The deviation of N2 from both N4 and N8 between 0 and 50° is likely due to the different basis sets employed.	16
A.3	N2, N4, and N8 absolute NICS 1_{ZZ} values as a function of torsion angle. The magnitude of NICS values decrease with chain length, and we expected that the values will converge once a certain chain length is reached. While the magnitude decreases the overall trend as a function of torsion angle is consistent, which allows N2 to represent larger chains.	17
A.4	Comparison of the aromaticity indexes MCI and NICS for BT.	18
A.5	Comparison of the aromaticity indexes MCI and NICS for hBT.	19
A.6	Comparison of the aromaticity indexes MCI and NICS for F2-BT.	20
A.7	Comparison of the aromaticity indexes MCI and NICS for BEDOT.	20
A.8	A potential energy scan of the interatomic separation distance between a hydrogen and a sulfur atom on thiophene molecules. The orange dot represents the relaxed H ··· S distance on a trans (180°) BT molecule. This indicates that the H ··· S through-space interaction is marginally repulsive in trans BT. It is noteworthy that the repulsive energy is small compared to the torsional barrier present at 180° in BT (a factor of ~2.5), which in combination with the NCI analysis below demonstrate the minor role of sterics in determining planarity.	21
A.9	The NCI analysis of BT including an NCI isosurface (right) and an $s(\rho)$ plot (center), which displays the reduced density gradient (RDG) as a function of the sign of the electron-density Hessian matrix's second eigenvalue ($\text{sign}(\lambda_2)$) times the electron-density (ρ). The isosurface plot on right shows a van der Waals interaction between H ··· S. The color gradient at the top gives a rough physical description of the color scheme used for the isosurface. When only the localized region around H ··· S is considered, by employing a radius cutoff, the $s(\rho)$ plot is inconclusive exhibiting both weakly repulsive and weakly attractive interactions.	22
A.10	A potential energy scan of the interatomic separation distance between a fluoride and a sulfur atom on a fluorinated thiophene and a thiophene molecule. The orange dot represents the relaxed F ··· S distance on a trans (180°) 3F-BT molecule. This indicates that the F ··· S through-space interaction is repulsive in trans 3F-BT.	23
A.11	A potential energy scan of the interatomic separation distance between a fluoride and a sulfur atom on a fluorinated thiophene molecules. The orange dot represents the relaxed F ··· S distance on a trans (180°) F2-BT molecule. This indicates that the F ··· S through-space interaction is repulsive in trans F2-BT.	24

A.12 The NCI analysis of F2-BT including an NCI isosurface (right) and an $s(\rho)$ plot (center), which displays the reduced density gradient (RDG) as a function of the sign of the electron-density Hessian matrix's second eigenvalue ($\text{sign}(\lambda_2)$) times the electron-density (ρ). The isosurface plot on right shows a van der Waals interaction between $\text{H} \cdots \text{S}$. The color gradient at the top gives a rough physical description of the color scheme used for the isosurface. When only the localized region around $\text{H} \cdots \text{S}$ is considered, by employing a radius cutoff, the $s(\rho)$ plot is inconclusive exhibiting both weakly repulsive and weakly attractive interactions.

25

A.13 A potential energy scan of the interatomic separation distance between a oxygen and a sulfur atom on an EDOT and thiophene molecule respectively. The thiophene molecule has been rotated such the ring is perpendicular to the EDOT ring, this is done to minimize secondary $\text{H} \cdots \text{S}$ interactions. The orange dot represents the relaxed $\text{O} \cdots \text{S}$ distance on a trans (180°) BEDOT molecule. This indicates that the $\text{O} \cdots \text{S}$ through-space interaction is repulsive in trans BEDOT.

26

A.14 The NCI analysis of BEDOT including an NCI isosurface (right) and an $s(\rho)$ plot (center), which displays the reduced density gradient (RDG) as a function of the sign of the electron-density Hessian matrix's second eigenvalue ($\text{sign}(\lambda_2)$) times the electron-density (ρ). The isosurface plot on right shows a van der Waals interaction between $\text{H} \cdots \text{S}$. The color gradient at the top gives a rough physical description of the color scheme used for the isosurface. When only the localized region around $\text{H} \cdots \text{S}$ is considered, by employing a radius cutoff, the $s(\rho)$ plot is inconclusive exhibiting both weakly repulsive and weakly attractive interactions.

27

List of Tables

Acknowledgments

Thank everyone here

Chapter 1

Introduction

Intro goes here

Chapter 2

Structural Changes in Doped and Excited Conjugated Polymers

first paper here

Chapter 3

Aromaticity as a Guide to Planarity in Conjugated Molecules and Polymers

3.1 Introduction

Organic semiconductors offer unique blends of physical and electronic properties along with the processability and fabrication potential of polymers and small molecules.[29, 37] This combination opens up countless opportunities for new functional materials that can be tailored for specific applications.[32, 33, 36, 38] One successful strategy for tuning molecular properties is adding pendent groups to the conjugated backbone; these “noncovalent locks” control molecular structure by inducing nonbonded interactions.[23, 3, 4, 21] The goal is to create structures that prefer coplanar torsional configurations that maximize electron delocalization across the molecule or polymer (i.e. conjugation), and as a result improve electronic properties such as carrier mobility.

While noncovalent locks have proven to be effective at creating planar structures, the exact nature of the interactions leading to planarity remain difficult to disentangle. A few reports have attempted to isolate and identify the fundamental interactions behind noncovalent locking systems. For instance, Jackson et al. demonstrated that nontraditional hydrogen bonding (i.e. hydrogen bonding that involves less electronegative atoms such as C, S, and Cl) can play a predominant role in stabilizing planar configurations.[23] Nevertheless, many locking molecules such as 3,4-ethylenedioxythiophene (EDOT) and fluorinated thiophenes—which are utilized in state-of-the-art conjugated molecules and polymers[41, 18, 40, 13, 14, 24, 30]—do not involve nontraditional hydrogen bonding. Conboy et al. confirmed the importance of heteroatom interactions in poly-EDOT (PEDOT) and similar molecules, but stated that a precise description of torsional energetics was unclear and speculated that electrostatics were responsible for the observed planarity.[4]

Aromaticity is a common chemical descriptor that can be used to simplify some of the underlying physics and provide novel insights into torsional energetics. A key objective of this communication is to highlight how the competition between aromaticity and conjugation[20,

[27, 21] influences planarity in organic electronic materials. We show that the introduction of popular noncovalent locks modifies aromaticity and drives structures towards planarity. Finally, we identify the specific hyperconjugation interaction that alters aromaticity and determines planarity.

3.2 Results and Discussion

An illustrative example of the balance between ring aromaticity and conjugation is the torsion potential of bithiophene (BT) (Fig. 3.1). Dimers provide a computationally efficient and accurate representation of the torsion potential and trends in aromaticity observed in larger conjugated polymers (See SI)[8] and hence are used throughout this work. The aromaticity of individual rings is quantified using the multicenter bonding index (MCI),[16, 15] and the nucleus-independent chemical shift (NICS)[9, 2] (see SI). We represent conjugation semi-quantitatively as the normalized relative bond length of the bridge C-C bond between rings; the rational being configurations with shorter bridge bonds are more conjugated.[7, 10] Figure 1 (left side) clearly shows that the stabilizing effects of aromaticity and conjugation are in direct competition with one another. This agrees with a simple description based on atomic orbitals, where planar structures (0° cis and 180° trans) exhibit the most p_z -orbital overlap (π -bonding) and afford the most electron delocalization across the molecule. Whereas the torsioned structure at 90° will exhibit the least electron sharing between rings, and it possesses the highest ring aromaticity or electron delocalization within a ring. The non-planar global minimum (150°) in the torsion potential appears to be the balance between these two driving forces.

To test this hypothesis we removed aromaticity by hydrogenating the terminal C=C double bonds, leaving intact the conjugation across the rings (right side of Fig. 3.1). Once aromaticity was removed the torsional energetics essentially mirrored conjugation, and most importantly the global minimum in the torsion potential shifted to the planar 180° configuration. It is noteworthy that the inter-ring H \cdots S distance is reduced in hydrogenated bithiophene (hBT) (2.78Å in the 180° configuration) compared to BT (2.93Å in the 180° configuration), which reduces concern that the 150° torsional minimum in BT is due to steric repulsion between H \cdots S. This conclusion is supported with through-space calculations and noncovalent interaction (NCI) analysis[25, 5] in the SI. Establishing aromaticity as a driving force in torsional energetics is fundamental for understanding structure; additionally, if aromaticity can be modified or controlled it may represent a design opportunity.

Having demonstrated the important role of aromaticity in directing torsion angles, we were motivated to explore the role of aromaticity in known planar systems with noncovalent locks. We discovered a number of reported noncovalent locks modify aromaticity. As observed in the top of Fig. 3.2 both 3,3'-difluorobithiophene (F2-BT) and bis-EDOT (BEDOT) exhibit a coplanar torsional minimum at 180° accompanied by an increase in aromaticity near 180° . As expected, conjugation is minimized at 90° and a maximized at 180° , it has been left out of Fig. 3.2 for clarity. For torsional energetics the magnitude of aromaticity is less important

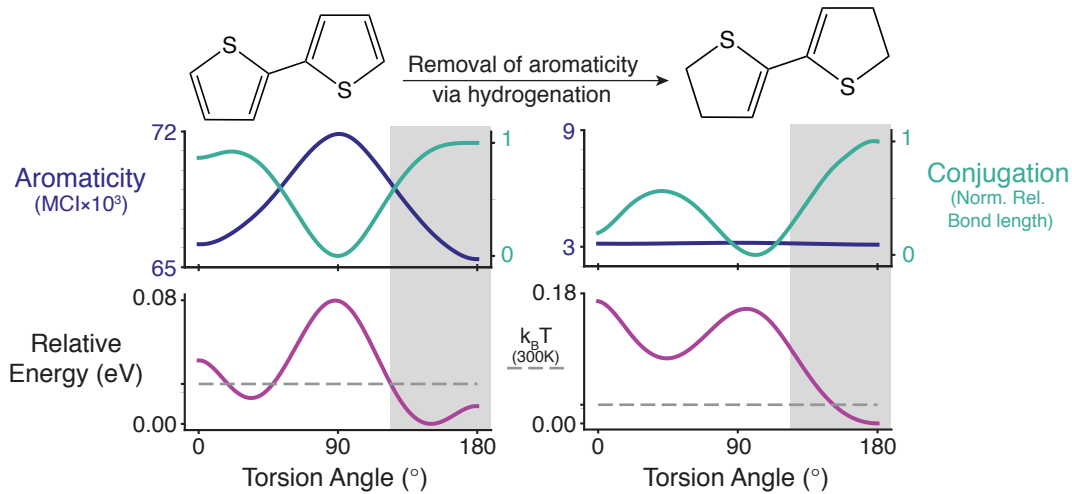


Figure 3.1: Ring aromaticity, molecular conjugation, and relative energies are plotted as a function of torsion angle for bithiophene (BT) and hydrogenated bithiophene (hBT). Both BT and hBT structures are represented in the 180° (trans) configuration. Aromaticity and conjugation are directly opposed in BT and the balance between the two driving forces results in a non-planar torsional minimum around 150°. Hydrogenation of the terminal C-C double bonds essentially reduces aromaticity to zero, while preserving conjugation across the two rings. With aromaticity removed in hBT, torsional energetics mirror conjugation and there is a planar minimum at 180°. Aromaticity is defined as the multicenter bonding index ($MCI \times 10^3$) for one C-C-S-C-C thiophene ring. Only one ring is displayed because both BT and hBT are symmetric molecules. Conjugation is quantified as the normalized relative bridge C-C bond length. A value of 1 represents the shortest bond length and the highest conjugation, whereas 0 represents the longest bond and lowest amount of conjugation.

than the change in aromaticity. For example, if aromaticity is constant across all torsion angles there is no torsional driving force. As a result, we are interested in the change in aromaticity between 90–180°.

To further investigate the modification of aromaticity we systematically added fluorine at different ring positions (bottom of Fig. 3.2). Notably, aromaticity increases near 180° in ring 2 (the ring without F added) of 3F-BT similarly to that of BEDOT and F2-BT in the top of Fig. 3.2. With only one added fluorine the aromaticity of both ring 1 and ring 2 need to be characterized because the molecule is no longer symmetric. When fluorine is added to ring 1—regardless of the position—it reduces the magnitude of aromaticity but preserves the shape of the curve (bottom left of Fig. 3.2), essentially reducing the underlying function by a constant. This is consistent with earlier reports that adding electron withdrawing substituents to an aromatic ring reduces the overall aromaticity.[28] Naively, one might expect all thiophene rings without F added to be similar, and this is largely true for ring 2 of BT and

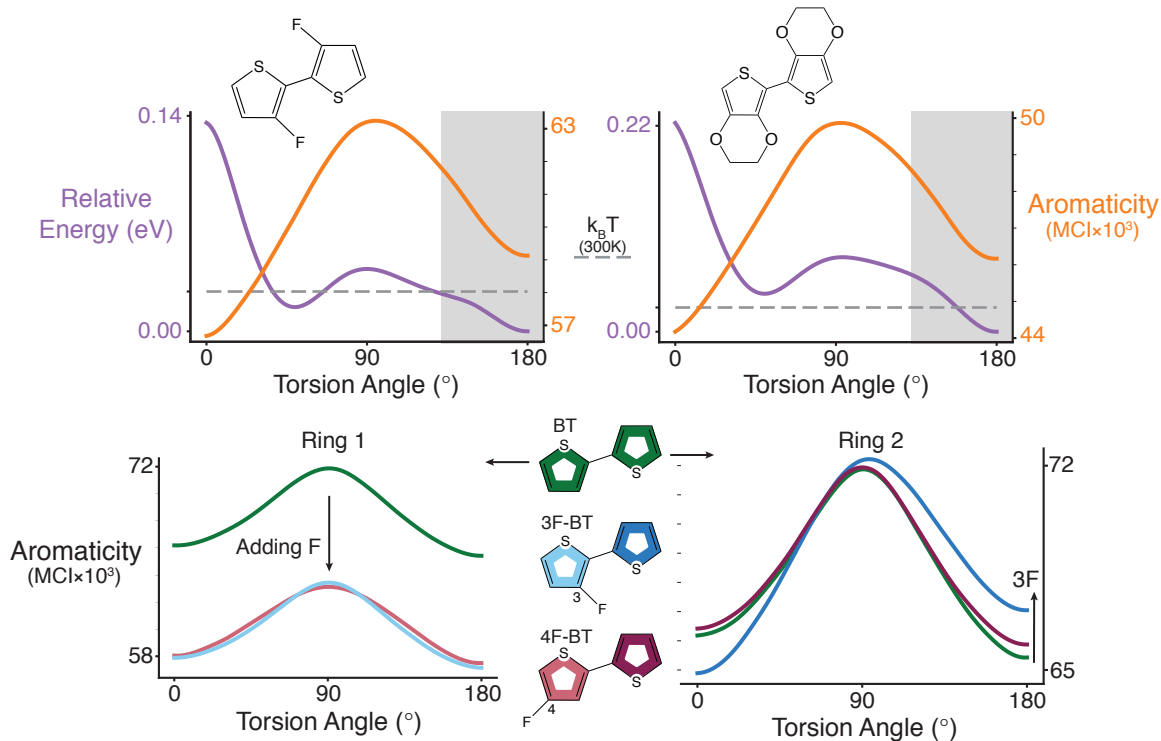


Figure 3.2: (Top) Torsional relative energies and aromaticity are plotted for F2-BT and BEDOT. In both systems aromaticity is increased near 180° and this corresponds to an energetic minimum. (Bottom) Ring 1 and ring 2 aromaticities are plotted against torsion angles for BT, 3F-BT, and 4F-BT. Both rings are plotted because 3F-BT and 4F-BT molecules are no longer symmetric as is BT. For ring 1 the addition of F—regardless of the position—reduces the magnitude of aromaticity by a constant, but preserves the shape of the BT curve. The ring 2 curves are similar for 4F-BT and BT, however, ring 2 of 3F-BT deviates in shape and aromaticity is increased near 180° similar to the plots in the top of figure.

4F-BT but as mentioned ring 2 aromaticity is modified in 3F-BT. This result indicates that there is a noncovalent inter-ring interaction between $F \cdots S$ causing the change in aromaticity.

Using Natural Bonding Orbital (NBO) analysis we identify the key interaction responsible for the modification of aromaticity and for stabilizing the planar 180° configuration (Fig. 3.3). Our through-space calculations for $F \cdots S$ and $O \cdots S$ indicate that both would be repulsive at the respective relaxed separation distance present in the 180° configuration of F2-BT and BEDOT (see SI). Thus, it is clear that some other interaction involving $X \cdots S$ is stabilizing the steric effects in order for the 180° configuration to be energetically favorable. NBO perturbation analyses revealed a 3-center-2-electron interaction between a heteroatom lone pair and a C-S antibonding orbital (σ_{C-S}^*) pictured in the top of Fig. 3.3. Details on specific

energies are provided in the SI. Similar interactions have been reported for the association of supramolecules.[6] Conboy et al. mentioned this type of interaction as a possible source of attraction in BEDOT-like molecules, but dismissed it due to a lack of bond length correlations across a series of related molecules.[4]

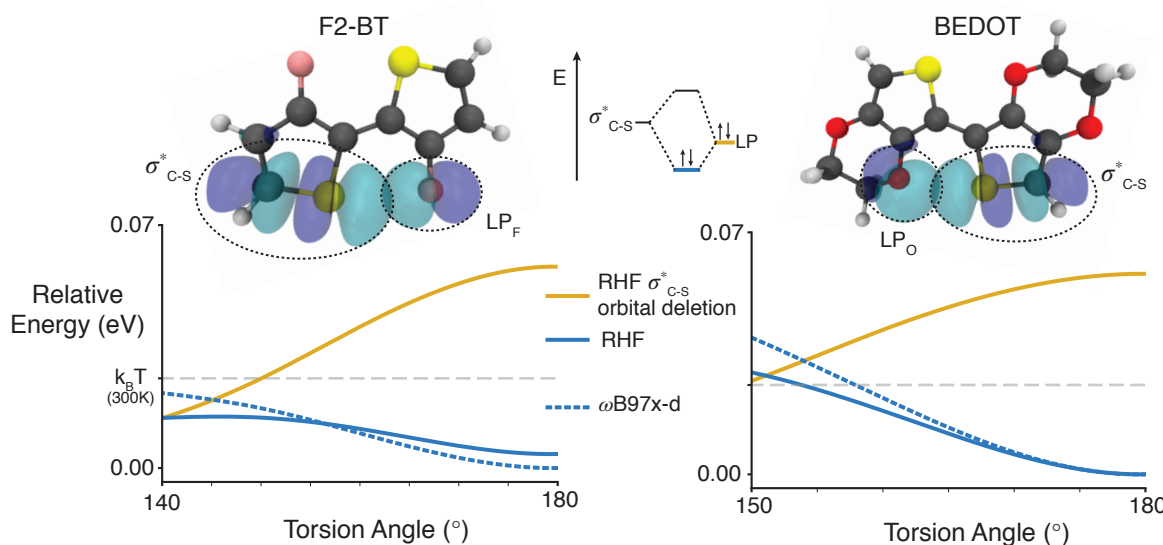


Figure 3.3: (Top) Isosurface plots of the overlap between C-S antibonding (σ^*_{C-S}) and F or O lone pair (LP) natural bonding orbitals in F2-BT and EDOT (isovalue ≈ 0.03). The orbital overlap leads to a stabilizing hyperconjugation interaction depicted in between the isosurface plots. (Bottom) The torsion potentials of F2-BT and BEDOT are displayed for ω B97x-D, RHF, and RHF with the σ^*_{C-S} orbital removed. RHF and ω B97x-D are qualitatively similar, both having a minimum at 180°. When the σ^*_{C-S} orbital is deleted from the Fock matrix (using NBO6) the hyperconjugative stabilization is no longer present and without that interaction the molecules are no longer planar.

In order to confirm the importance of the 3-center-2-electron interaction we utilized the NBO deletion method[17], which has been used previously to deconvolute torsional energetics.[34] Because the NBO deletion method necessitates the use of restricted Hartree-Fock (RHF) we recalculated the torsion potentials with RHF to ensure qualitatively similar behavior to the higher level of theory (ω B97x-D). Then using the RHF deletion method, we removed the C-S antibonding orbitals (σ^*_{C-S}) on both rings, which eliminates hyperconjugation. Remarkably, removing hyperconjugation altered the torsional energetics in both BEDOT and F2-BT such that the planar 180° configurations are no longer favorable (as shown in Figure 3), most likely due to the steric repulsion that exists. We characterize these as hyperconjugation interactions because they result in electron delocalization across the molecule and there is a history of hyperconjugation impacting torsional energetics.[34, 35] This result provides strong

evidence that hyperconjugation is the critical interaction responsible for the locking behavior in these molecules and polymers.

3.3 Conclusion

Using a variety of computational techniques we have demonstrated that aromaticity is a useful descriptor to help understand the complex interactions which lead to the structure of conjugated molecules and polymers. In general, aromaticity is stabilizing and energetically favorable, and in extended conjugated molecules and polymers ring aromaticity prefers torsioned or non-planar configurations because it confines delocalized electrons within a ring instead of delocalizing them across the entire molecule or polymer. As such, aromaticity directly competes with conjugation, also known to be stabilizing and energetically favorable. BT is an ideal system to exemplify this competition, and ultimately we identify a balance between the two factors that results in a non-planar minimum energy configuration. Planarity and conjugation are vital for the electronic properties of conjugated materials so minimizing the driving force from aromaticity is industrially relevant. We find that aromaticity can indeed be beneficially modified through pendent group additions or noncovalent locks such as F2-BT and BEDOT. In both examples, a heteroatom interacts with an adjacent ring and increases its aromaticity at torsional angles near 180° where the atoms are the closest together. To probe the exact nature of this interaction we identified and removed hyperconjugation between a heteroatom (i.e. F and O) lone pair and the C-S antibonding orbital on the adjacent ring, concluding that hyperconjugation is responsible for the changes in aromaticity and for the resulting planarity or locking behavior. We anticipate that the structural insights and methods presented here are applicable to a wide range of conjugated molecules and polymers, and will open the door to new and unforeseen advances in our ability to design functional organic electronic materials.

3.4 Computational Methods

All quantum chemistry calculations were performed with Gaussian 16 unless otherwise noted.^[12] The default level of theory was ω B97x-D with the def2-TZVPP basis set.^[1, 39] The general procedure for calculating torsion potentials started with an unconstrained geometry relaxation followed by a frequency calculation to ensure no substantial imaginary frequencies existed. Then the relaxed geometry was rotated around the central C-C bond, fixing the C-C-C-C torsion every 10° for a constrained geometry optimization. An additional torsional constraint was used for hydrogenated calculations (See SI). MCI aromaticities were computed with the natural atomic orbital basis from NBO6 for all 5 member (C-C-S-C-C) rings at each torsional geometry using Multiwfn.^[31] NBO analysis was performed using NBO6.^[17] All RHF and RHF NBO orbital deletions were done with Gaussian 09^[11] and NBO6 again using the def2-TZVPP basis set. RHF NBO orbital deletions were single point calculations utilizing

relaxed RHF geometries. Isosurface images were made with VMD,[22] and all plotting utilized Matplotlib and cubic spline interpolation via SciPy.[26]

Chapter 4

Conclusion

Conclude here

Bibliography

- [1] Jeng-Da Chai and Martin Head-Gordon. “Long-range corrected hybrid density functionals with damped atom-atom dispersion corrections”. In: *Physical Chemistry Chemical Physics* 10.44 (2008), p. 6615. ISSN: 1463-9076. DOI: [10.1039/b810189b](https://doi.org/10.1039/b810189b). arXiv: [1211.0387](https://arxiv.org/abs/1211.0387). URL: <http://xlink.rsc.org/?DOI=b810189b>.
- [2] Zhongfang Chen et al. “Nucleus-Independent Chemical Shifts (NICS) as an Aromaticity Criterion”. In: *Chemical Reviews* 105.10 (2005), pp. 3842–3888. DOI: [10.1021/cr030088+](https://doi.org/10.1021/cr030088+).
- [3] Yuanfang Cheng et al. “Controlling Intramolecular Conformation through Nonbonding Interaction for Soft-Conjugated Materials: Molecular Design and Optoelectronic Properties”. In: *Journal of Physical Chemistry Letters* 7.18 (2016), pp. 3609–3615. ISSN: 19487185. DOI: [10.1021/acs.jpclett.6b01695](https://doi.org/10.1021/acs.jpclett.6b01695).
- [4] Gary Conboy et al. “To bend or not to bend - are heteroatom interactions within conjugated molecules effective in dictating conformation and planarity?” In: *Material Horizons* 3.4 (2016), pp. 333–339. DOI: [10.1039/c6mh00051g](https://doi.org/10.1039/c6mh00051g).
- [5] Julia Contreras-García et al. “NCIPILOT: A program for plotting noncovalent interaction regions”. In: *Journal of Chemical Theory and Computation* 7.3 (2011), pp. 625–632. ISSN: 15499618. DOI: [10.1021/ct100641a](https://doi.org/10.1021/ct100641a). arXiv: [9504352 \[hep-ph\]](https://arxiv.org/abs/9504352).
- [6] Anthony F. Cozzolino et al. “The nature of the supramolecular association of 1,2,5-chalcogenadiazoles”. In: *Journal of the American Chemical Society* 127.9 (2005), pp. 3184–3190. ISSN: 00027863. DOI: [10.1021/ja044005y](https://doi.org/10.1021/ja044005y).
- [7] J. P. Daudey et al. “Decisive role of π conjugation in the central bond length shortening of butadiene”. In: *Tetrahedron* 36.23 (1980), pp. 3399–3401. ISSN: 0040-4020. DOI: [10.1016/0040-4020\(80\)80190-6](https://doi.org/10.1016/0040-4020(80)80190-6).
- [8] Kateri H. Dubay et al. “Accurate Force Field Development for Modeling Conjugated Polymers”. In: *Journal of Chemical Theory and Computation* 8.11 (2012), pp. 4556–4569. ISSN: 15499618. DOI: [10.1021/ct300175w](https://doi.org/10.1021/ct300175w).
- [9] Hossein Fallah-Bagher-Shaiedaei et al. “Which NICS aromaticity index for planar π rings is best?” In: *Organic Letters* 8.5 (2006), pp. 863–866. ISSN: 15237060. DOI: [10.1021/o10529546](https://doi.org/10.1021/o10529546).

- [10] Israel Fernández and Gernot Frenking. “Direct estimate of the strength of conjugation and hyperconjugation by the energy decomposition analysis method”. In: *Chemistry - A European Journal* 12.13 (2006), pp. 3617–3629. ISSN: 09476539. DOI: [10.1002/chem.200501405](https://doi.org/10.1002/chem.200501405).
- [11] M. J. Frisch et al. *Gaussian09 Revision D.01*. Gaussian Inc. Wallingford CT. 2009.
- [12] M. J. Frisch et al. *Gaussian16 Revision A.03*. Gaussian Inc. Wallingford CT. 2016.
- [13] Yao Gao et al. “High Mobility Ambipolar Diketopyrrolopyrrole-Based Conjugated Polymer Synthesized Via Direct Arylation Polycondensation”. In: *Advanced Materials* 27.42 (2015), pp. 6753–6759. ISSN: 15214095. DOI: [10.1002/adma.201502896](https://doi.org/10.1002/adma.201502896).
- [14] Yao Gao et al. “High Mobility Ambipolar Diketopyrrolopyrrole-Based Conjugated Polymers Synthesized via Direct Arylation Polycondensation: Influence of Thiophene Moieties and Side Chains”. In: *Macromolecules* 51.21 (2018), pp. 8752–8760. ISSN: 15205835. DOI: [10.1021/acs.macromol.8b01112](https://doi.org/10.1021/acs.macromol.8b01112).
- [15] M. Giambiagi et al. “Multicenter bond indices as a measure of aromaticity”. In: *Physical Chemistry Chemical Physics* 2.15 (2000), pp. 3381–3392. ISSN: 14639076. DOI: [10.1039/b002009p](https://doi.org/10.1039/b002009p).
- [16] Mario Giambiagi, Myriam S. de Giambiagi, and Kleber C. Mundim. “Definition of a multicenter bond index”. In: *Structural Chemistry* 1.5 (1990), pp. 423–427. ISSN: 10400400. DOI: [10.1007/BF00671228](https://doi.org/10.1007/BF00671228).
- [17] E. D. Glendening et al. *NBO 6.0*. Theoretical Chemistry Institute, University of Wisconsin, Madison, WI. 2013. URL: <http://nbo6.chem.wisc.edu/>.
- [18] Magnus Granstrom, Magnus Berggren, and Olle Inganäs. “Micrometer- and Nanometer-Sized Polymeric Light-Emitting Diodes”. In: *Science* 267.5203 (1995), pp. 1479–1481. DOI: [10.1126/science.267.5203.1479](https://doi.org/10.1126/science.267.5203.1479).
- [19] W J Hehre, R Ditchfield, and J A Pople. “Self-Consistent Molecular Orbital Methods . XII . Further Extensions of Gaussian-Type Basis Sets for Use in Molecular Orbital Studies of Organic Molecules”. In: 56.5 (1972), pp. 2257–2261. DOI: [10.1063/1.1677527](https://doi.org/10.1063/1.1677527).
- [20] V. Hernandez et al. “Confinement potential and π -electron delocalization in polyconjugated organic materials”. In: *Physical Review B* 50.14 (1994), pp. 9815–9823. ISSN: 01631829. DOI: [10.1103/PhysRevB.50.9815](https://doi.org/10.1103/PhysRevB.50.9815).
- [21] Hui Huang et al. “Organic and Polymeric Semiconductors Enhanced by Noncovalent Conformational Locks”. In: *Chemical Reviews* 117.15 (2017), pp. 10291–10318. ISSN: 15206890. DOI: [10.1021/acs.chemrev.7b00084](https://doi.org/10.1021/acs.chemrev.7b00084).
- [22] William Humphrey, Andrew Dalke, and Klaus Schulten. “VMD – Visual Molecular Dynamics”. In: *Journal of Molecular Graphics* 14 (1996), pp. 33–38.
- [23] Nicholas E Jackson et al. “Controlling Conformations of Conjugated Polymers and Small Molecules: The Role of Nonbonding Interactions”. In: *Journal of the American Chemical Society* 135.28 (2013), pp. 10475–10483. DOI: [10.1021/ja403667s](https://doi.org/10.1021/ja403667s).

- [24] Jea Woong Jo et al. "Fluorination of polythiophene derivatives for high performance organic photovoltaics". In: *Chemistry of Materials* 26.14 (2014), pp. 4214–4220. ISSN: 15205002. DOI: [10.1021/cm502229k](https://doi.org/10.1021/cm502229k).
- [25] Erin R. Johnson et al. "Revealing Noncovalent Interactions". In: *Journal of the American Chemical Society* 132.18 (2010), pp. 6498–6506. ISSN: 0002-7863. DOI: [10.1021/ja100936w](https://doi.org/10.1021/ja100936w).
- [26] Eric Jones, Travis Oliphant, Pearu Peterson, et al. *SciPy: Open source scientific tools for Python*. 2001–. URL: <http://www.scipy.org/>.
- [27] Miklos Kertesz, Cheol Ho Choi, and Shujiang Yang. "Conjugated polymers and aromaticity". In: *Chemical Reviews* 105.10 (2005), pp. 3448–3481. ISSN: 00092665. DOI: [10.1021/cr990357p](https://doi.org/10.1021/cr990357p).
- [28] Tadeusz M. Krygowski et al. "Aromaticity from the Viewpoint of Molecular Geometry: Application to Planar Systems". In: *Chemical Reviews* 114.12 (2014), pp. 6383–6422. ISSN: 0009-2665. DOI: [10.1021/cr400252h](https://doi.org/10.1021/cr400252h).
- [29] Brooke Kuei and Enrique D. Gomez. "Chain conformations and phase behavior of conjugated polymers". In: *Soft Matter* 13.1 (2017), pp. 49–67. ISSN: 17446848. DOI: [10.1039/C6SM00979D](https://doi.org/10.1039/C6SM00979D).
- [30] Zhengke Li et al. "Dramatic performance enhancement for large bandgap thick-film polymer solar cells introduced by a difluorinated donor unit". In: *Nano Energy* 15 (2015), pp. 607–615. ISSN: 22112855. DOI: [10.1016/j.nanoen.2015.05.016](https://doi.org/10.1016/j.nanoen.2015.05.016). URL: <http://dx.doi.org/10.1016/j.nanoen.2015.05.016>.
- [31] Tian Lu and Feiwu Chen. "Multiwfn: A multifunctional wavefunction analyzer". In: *Journal of Computational Chemistry* 33.5 (2012), pp. 580–592. ISSN: 01928651. DOI: [10.1002/jcc.22885](https://doi.org/10.1002/jcc.22885).
- [32] Jianguo Mei et al. "Integrated materials design of organic semiconductors for field-effect transistors". In: *Journal of the American Chemical Society* 135.18 (2013), pp. 6724–6746. ISSN: 15205126. DOI: [10.1021/ja400881n](https://doi.org/10.1021/ja400881n).
- [33] Simon Muench et al. "Polymer-Based Organic Batteries". In: *Chemical Reviews* 116.16 (2016), pp. 9438–9484. ISSN: 15206890. DOI: [10.1021/acs.chemrev.6b00070](https://doi.org/10.1021/acs.chemrev.6b00070).
- [34] V. Pophristic and L. Goodman. "Hyperconjugation not steric repulsion leads to the staggered structure of ethane". In: *Nature* 411.6837 (2001), pp. 565–568. ISSN: 00280836. DOI: [10.1038/35079036](https://doi.org/10.1038/35079036).
- [35] Paul R. Rablen et al. "Is hyperconjugation responsible for the "gauche effect" in 1-fluoropropane and other 2-substituted-1-fluoroethanes?" In: *J. Chem. Soc., Perkin Trans. 2* 8 (1999), pp. 1719–1726. ISSN: 0300-9580. DOI: [10.1039/a901974j](https://doi.org/10.1039/a901974j).
- [36] Takao Someya, Zhenan Bao, and George G. Malliaras. "The rise of plastic bioelectronics". In: *Nature* 540.7633 (2016), pp. 379–385. ISSN: 14764687. DOI: [10.1038/nature21004](https://doi.org/10.1038/nature21004).

- [37] Timothy M. Swager. “50th Anniversary Perspective: Conducting/Semiconducting Conjugated Polymers. A Personal Perspective on the Past and the Future”. In: *Macromolecules* 50.13 (2017), pp. 4867–4886. ISSN: 0024-9297. DOI: [10.1021/acs.macromol.7b00582](https://doi.org/10.1021/acs.macromol.7b00582). URL: <http://pubs.acs.org/doi/abs/10.1021/acs.macromol.7b00582>.
- [38] Yoeri Van De Burgt et al. “Organic electronics for neuromorphic computing”. In: *Nature Electronics* 1.7 (2018), pp. 386–397. ISSN: 25201131. DOI: [10.1038/s41928-018-0103-3](https://doi.org/10.1038/s41928-018-0103-3). URL: <http://dx.doi.org/10.1038/s41928-018-0103-3>.
- [39] Florian Weigend and Reinhart Ahlrichs. “Balanced basis sets of split valence, triple zeta valence and quadruple zeta valence quality for H to Rn: Design and assessment of accuracy”. In: *Phys. Chem. Chem. Phys.* 7.18 (2005), pp. 3297–3305. DOI: [10.1039/b508541a](https://doi.org/10.1039/b508541a). URL: <http://dx.doi.org/10.1039/b508541a>.
- [40] Yair Haim Wijsboom et al. “Tuning of electronic properties and rigidity in PEDOT analogs”. In: *Journal of Materials Chemistry* 21.5 (2011), pp. 1368–1372. ISSN: 09599428. DOI: [10.1039/c0jm02679d](https://doi.org/10.1039/c0jm02679d).
- [41] Seungjib Yum et al. “Benzotriazole-containing planar conjugated polymers with non-covalent conformational locks for thermally stable and efficient polymer field-effect transistors”. In: *Chemistry of Materials* 26.6 (2014), pp. 2147–2154. ISSN: 15205002. DOI: [10.1021/cm4042346](https://doi.org/10.1021/cm4042346).

Appendix A

Appendix for Aromaticity as a Guide to Planarity in Conjugated Molecules and Polymers

A.1 Different Length Polymer Chains

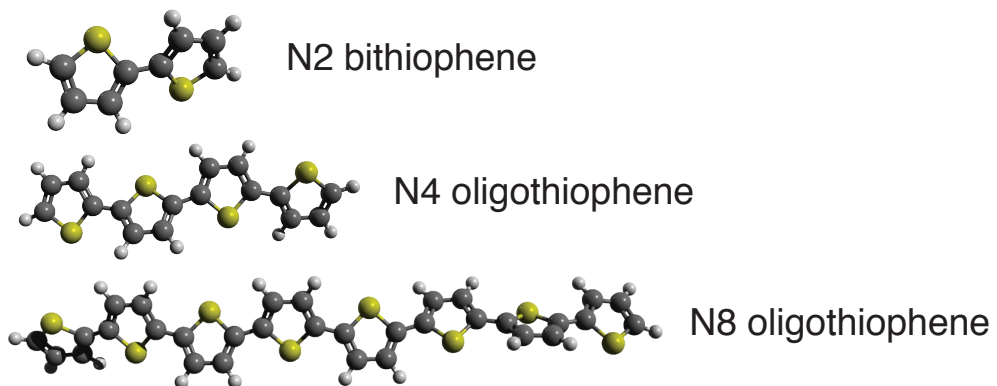


Figure A.1: Different length oligomers of thiophene.

Comparison of Torsion Potentials

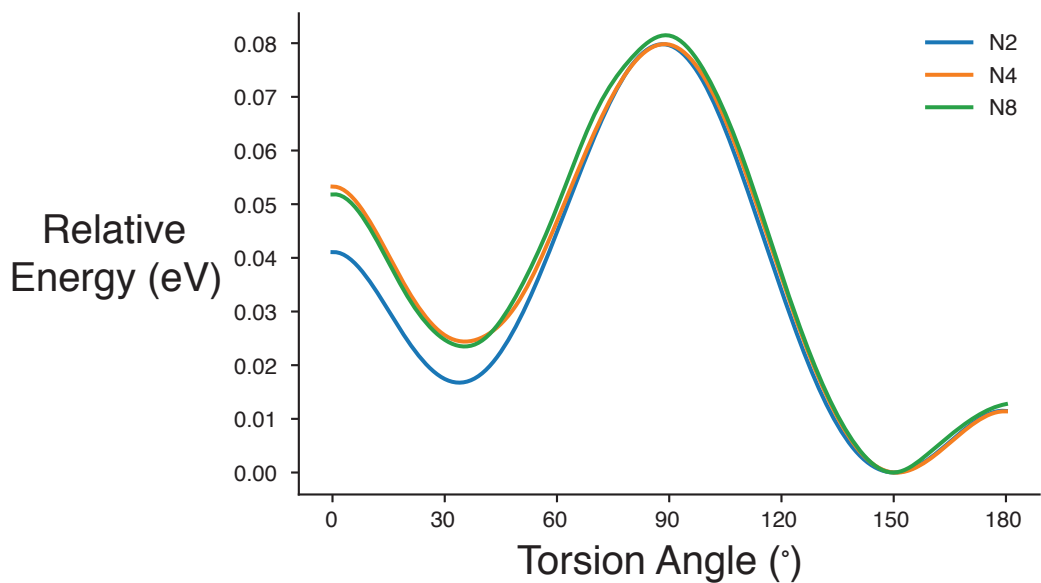


Figure A.2: The torsion potential of N2, N4, and N8 thiophene oligomers. All calculations were performed using the ω B97x-D functional. The N2 torsion potential was calculated with the def2-TZVPP basis set, while N4 and N8 utilized the 6-31++G**[19] basis set to reduce to the computational cost. The deviation of N2 from both N4 and N8 between 0 and 50° is likely due to the different basis sets employed.

Comparison of NICS Aromaticity

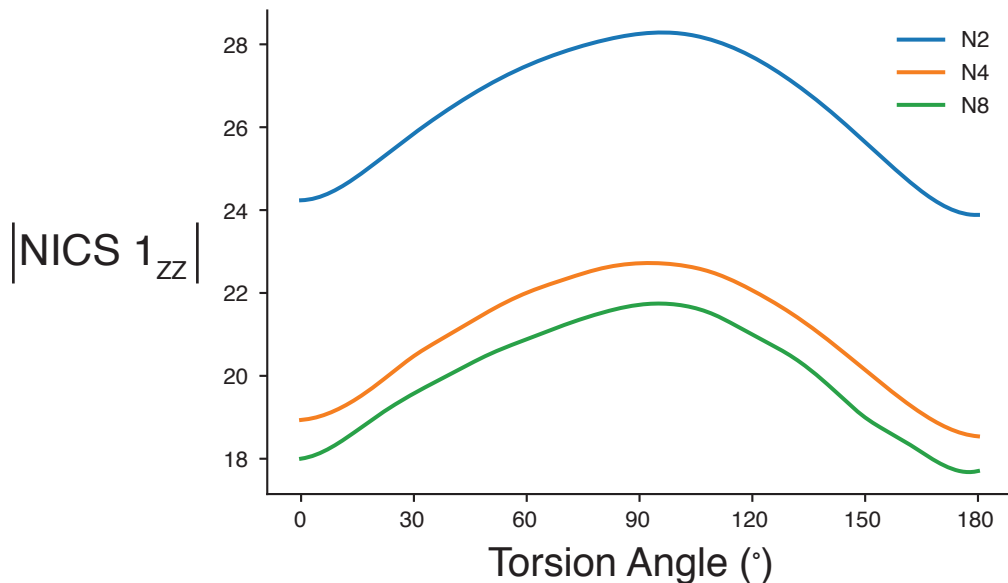


Figure A.3: N2, N4, and N8 absolute NICS 1_{zz} values as a function of torsion angle. The magnitude of NICS values decrease with chain length, and we expected that the values will converge once a certain chain length is reached. While the magnitude decreases the overall trend as a function of torsion angle is consistent, which allows N2 to represent larger chains.

A.2 Comparision of MCI and NICS Aromaticity Values

BT

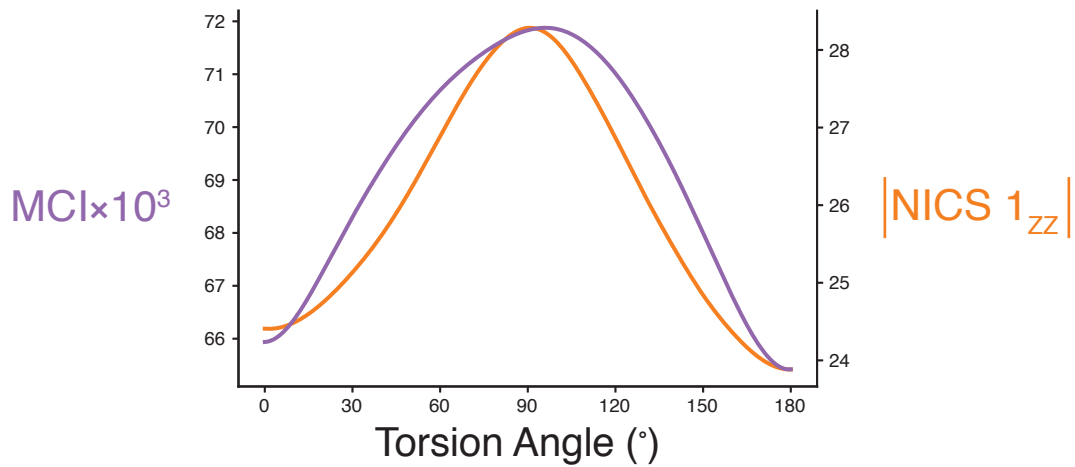


Figure A.4: Comparison of the aromaticity indexes MCI and NICS for BT.

hBT

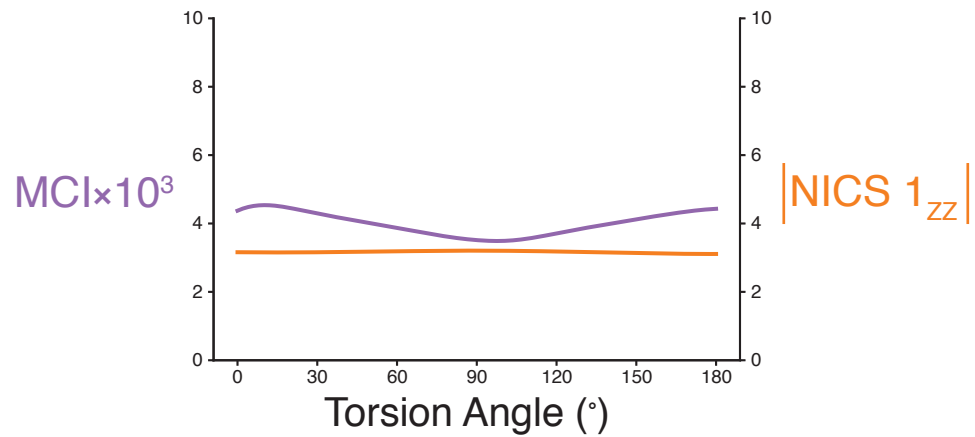


Figure A.5: Comparison of the aromaticity indexes MCI and NICS for hBT.

F2-BT

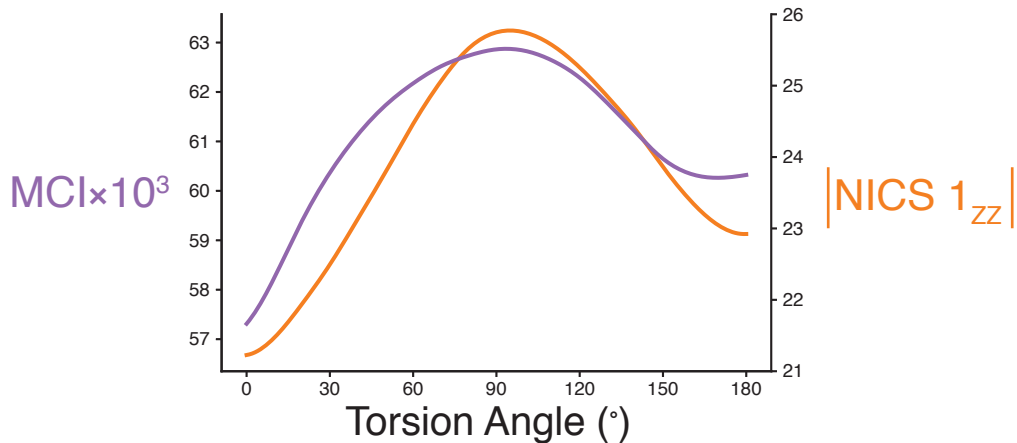


Figure A.6: Comparison of the aromaticity indexes MCI and NICS for F2-BT.

BEDOT

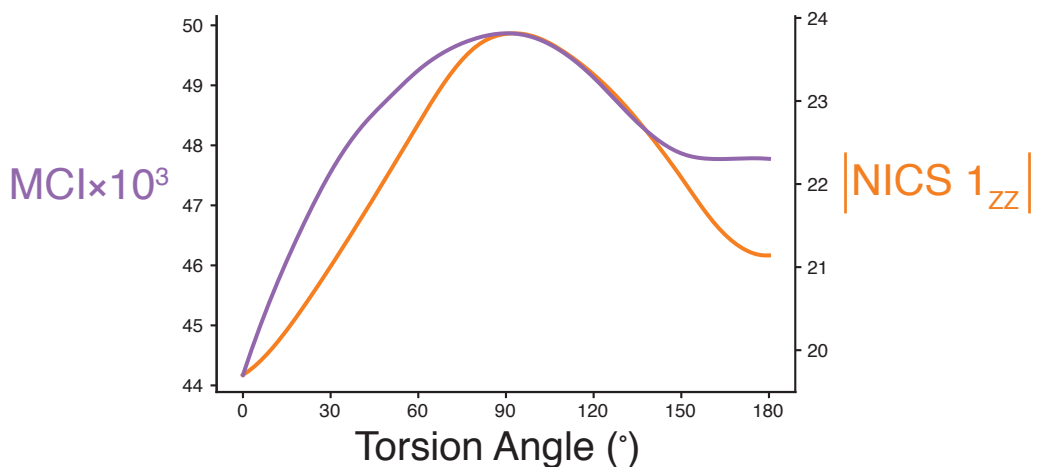


Figure A.7: Comparison of the aromaticity indexes MCI and NICS for BEDOT.

A.3 Through-space Calculations

$\text{H} \cdots \text{S}$

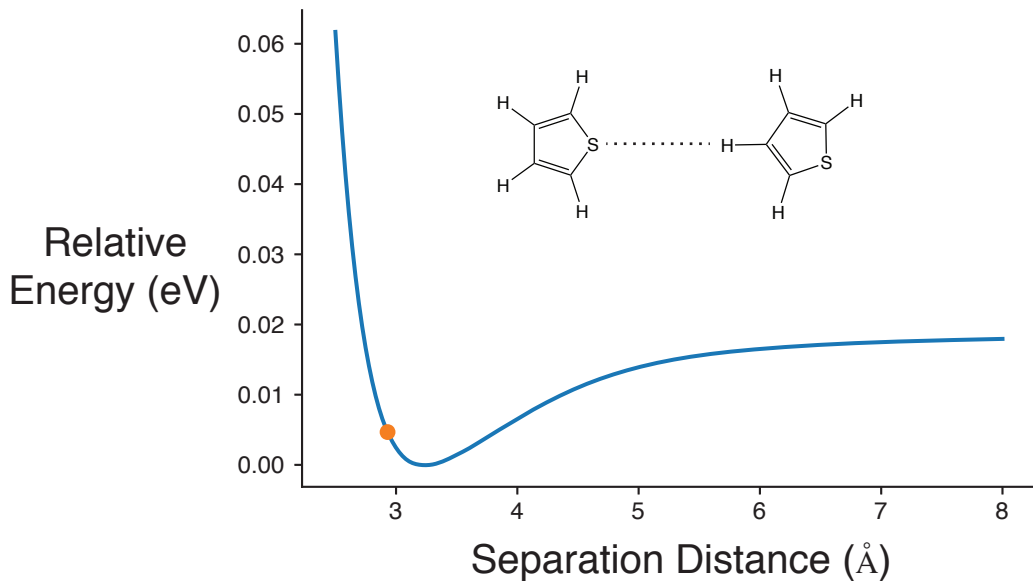


Figure A.8: A potential energy scan of the interatomic separation distance between a hydrogen and a sulfur atom on thiophene molecules. The orange dot represents the relaxed $\text{H} \cdots \text{S}$ distance on a trans (180°) BT molecule. This indicates that the $\text{H} \cdots \text{S}$ through-space interaction is marginally repulsive in trans BT. It is noteworthy that the repulsive energy is small compared to the torsional barrier present at 180° in BT (a factor of ~ 2.5), which in combination with the NCI analysis below demonstrate the minor role of sterics in determining planarity.

H ··· S Noncovalent Interaction Analysis

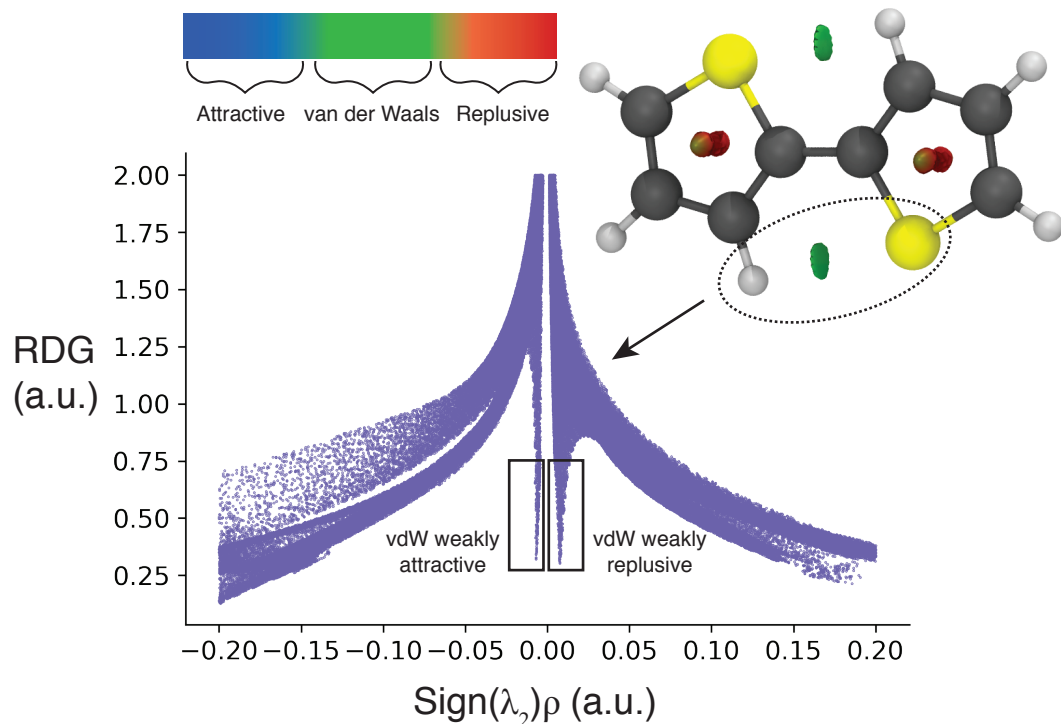


Figure A.9: The NCI analysis of BT including an NCI isosurface (right) and an $s(\rho)$ plot (center), which displays the reduced density gradient (RDG) as a function of the sign of the electron-density Hessian matrix's second eigenvalue ($\text{sign}(\lambda_2)$) times the electron-density (ρ). The isosurface plot on right shows a van der Waals interaction between $\text{H} \cdots \text{S}$. The color gradient at the top gives a rough physical description of the color scheme used for the isosurface. When only the localized region around $\text{H} \cdots \text{S}$ is considered, by employing a radius cutoff, the $s(\rho)$ plot is inconclusive exhibiting both weakly repulsive and weakly attractive interactions.

F ... S

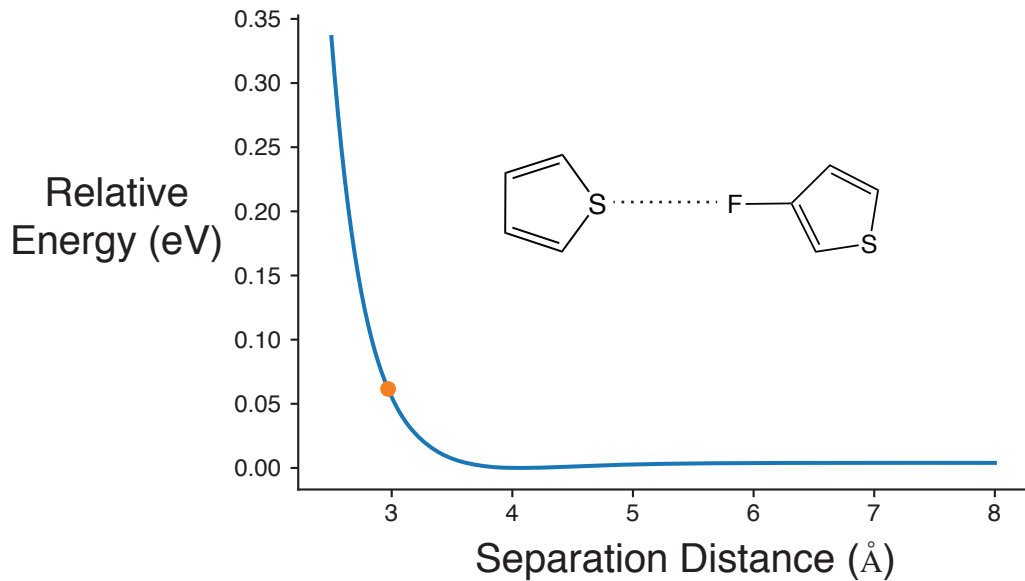


Figure A.10: A potential energy scan of the interatomic separation distance between a fluoride and a sulfur atom on a fluorinated thiophene and a thiophene molecule. The orange dot represents the relaxed $\text{F} \cdots \text{S}$ distance on a trans (180°) 3F-BT molecule. This indicates that the $\text{F} \cdots \text{S}$ through-space interaction is repulsive in trans 3F-BT.

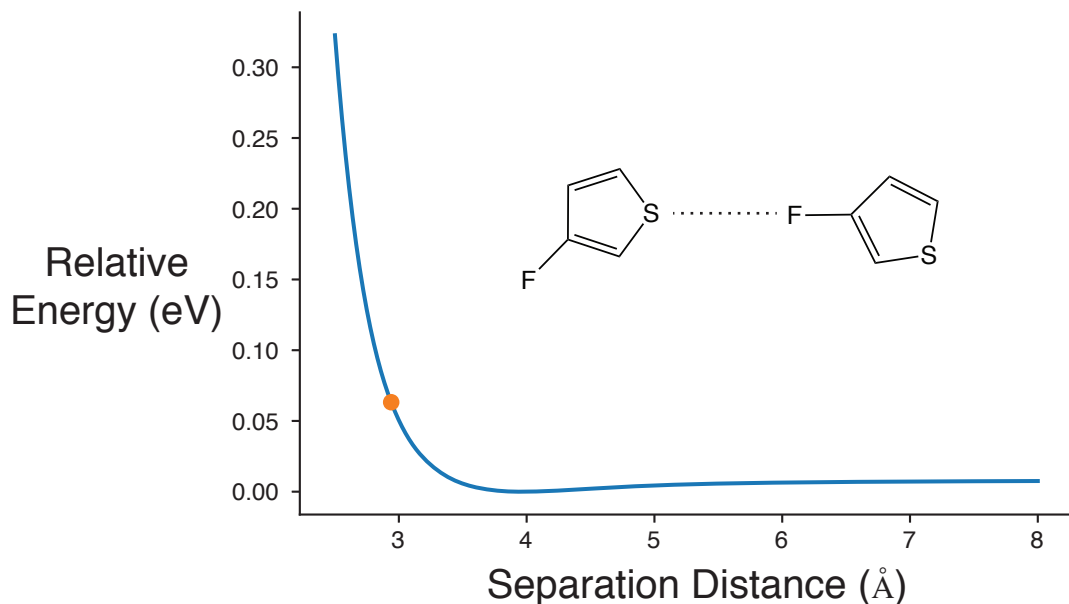


Figure A.11: A potential energy scan of the interatomic separation distance between a fluoride and a sulfur atom on a fluorinated thiophene molecules. The orange dot represents the relaxed $\text{F} \cdots \text{S}$ distance on a trans (180°) $\text{F}_2\text{-BT}$ molecule. This indicates that the $\text{F} \cdots \text{S}$ through-space interaction is repulsive in trans $\text{F}_2\text{-BT}$.

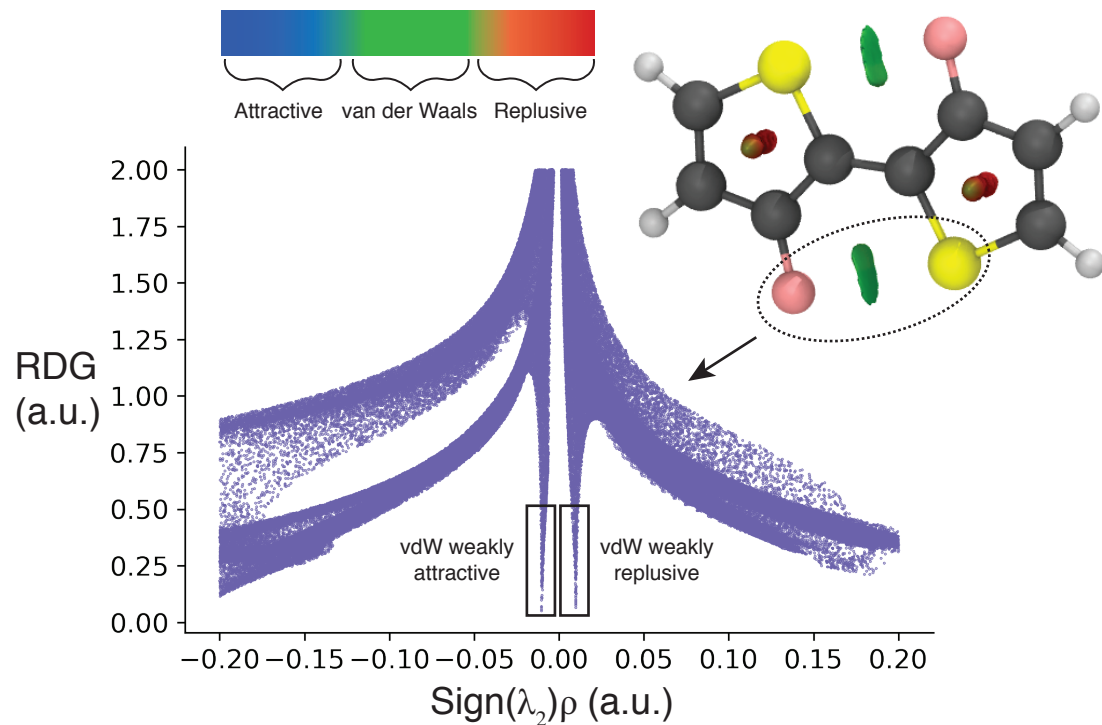
F . . . S Noncovalent Interaction Analysis


Figure A.12: The NCI analysis of F2-BT including an NCI isosurface (right) and an $s(\rho)$ plot (center), which displays the reduced density gradient (RDG) as a function of the sign of the electron-density Hessian matrix's second eigenvalue ($\text{sign}(\lambda_2)$) times the electron-density (ρ). The isosurface plot on right shows a van der Waals interaction between $H \cdots S$. The color gradient at the top gives a rough physical description of the color scheme used for the isosurface. When only the localized region around $H \cdots S$ is considered, by employing a radius cutoff, the $s(\rho)$ plot is inconclusive exhibiting both weakly repulsive and weakly attractive interactions.

O ... S

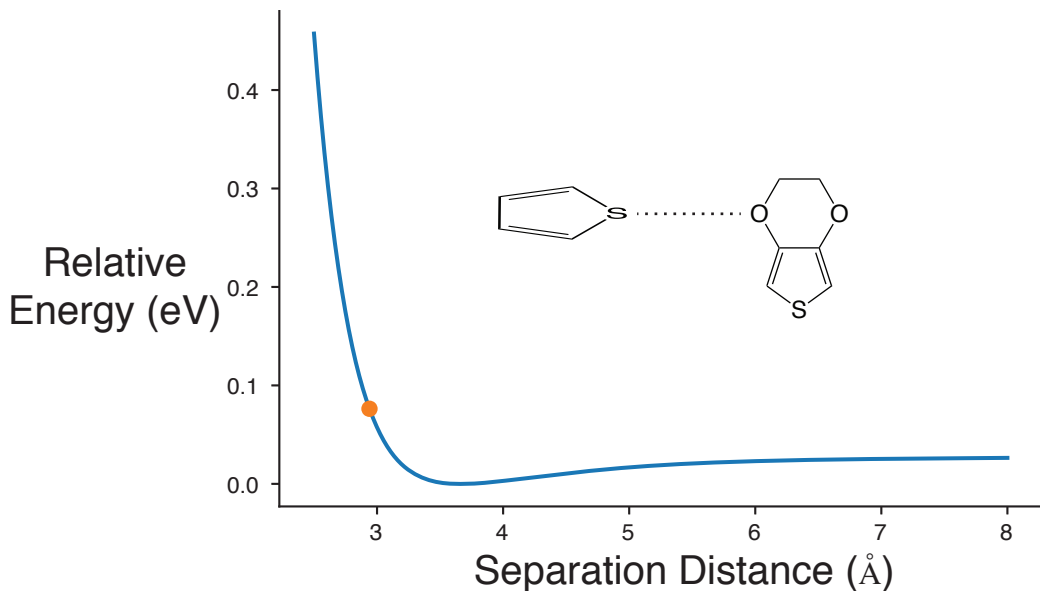


Figure A.13: A potential energy scan of the interatomic separation distance between a oxygen and a sulfur atom on an EDOT and thiophene molecule respectively. The thiophene molecule has been rotated such the ring is perpendicular to the EDOT ring, this is done to minimize secondary H ... S interactions. The orange dot represents the relaxed O ... S distance on a trans (180°) BEDOT molecule. This indicates that the O ... S through-space interaction is repulsive in trans BEDOT.

O ... S Noncovalent Interaction Analysis

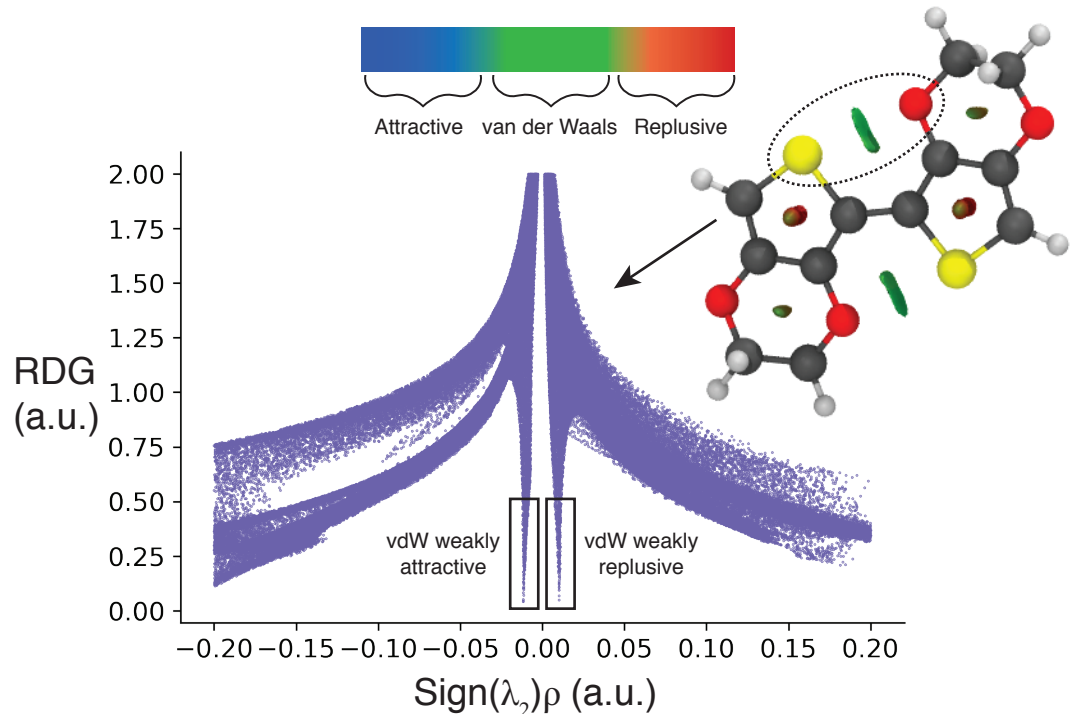


Figure A.14: The NCI analysis of BEDOT including an NCI isosurface (right) and an $s(\rho)$ plot (center), which displays the reduced density gradient (RDG) as a function of the sign of the electron-density Hessian matrix's second eigenvalue ($\text{sign}(\lambda_2)$) times the electron-density (ρ). The isosurface plot on right shows a van der Waals interaction between $\text{H} \cdots \text{S}$. The color gradient at the top gives a rough physical description of the color scheme used for the isosurface. When only the localized region around $\text{H} \cdots \text{S}$ is considered, by employing a radius cutoff, the $s(\rho)$ plot is inconclusive exhibiting both weakly repulsive and weakly attractive interactions.